JCI The Journal of Clinical Investigation

Vascular rarefaction mediates whitening of brown fat in obesity

Ippei Shimizu, Tamar Aprahamian, Ryosuke Kikuchi, Ayako Shimizu, Kyriakos N. Papanicolaou, Susan MacLauchlan, Sonomi Maruyama, Kenneth Walsh

Research Article   **Endocrinology**

Brown adipose tissue (BAT) is a highly vascularized organ with abundant mitochondria that produce heat through uncoupled respiration. Obesity is associated with a reduction of BAT function; however, it is unknown how obesity promotes dysfunctional BAT. Here, using a murine model of diet-induced obesity, we determined that obesity causes capillary rarefaction and functional hypoxia in BAT, leading to a BAT "whitening" phenotype that is characterized by mitochondrial dysfunction, lipid droplet accumulation, and decreased expression of *Vegfa*. Targeted deletion of *Vegfa* in adipose tissue of nonobese mice resulted in BAT whitening, supporting a role for decreased vascularity in obesity-associated BAT. Conversely, introduction of VEGF-A specifically into BAT of obese mice restored vascularity, ameliorated brown adipocyte dysfunction, and improved insulin sensitivity. The capillary rarefaction in BAT that was brought about by obesity or *Vegfa* ablation diminished β-adrenergic signaling, increased mitochondrial ROS production, and promoted mitophagy. These data indicate that overnutrition leads to the development of a hypoxic state in BAT, causing it to whiten through mitochondrial dysfunction and loss. Furthermore, these results link obesity-associated BAT whitening to impaired systemic glucose metabolism.

Find the latest version:

https://jci.me/71643/pdf

Vascular rarefaction mediates whitening of brown fat in obesity

Ippei Shimizu,[1] Tamar Aprahamian,[1,2] Ryosuke Kikuchi,[1] Ayako Shimizu,[1]
Kyriakos N. Papanicolaou,[1] Susan MacLauchlan,[1] Sonomi Maruyama,[1] and Kenneth Walsh[1]

[1]Molecular Cardiology and Whitaker Cardiovascular Institute, and [2]Department of Medicine–Renal Section,
Boston University School of Medicine, Boston, Massachusetts, USA.

Brown adipose tissue (BAT) is a highly vascularized organ with abundant mitochondria that produce heat through uncoupled respiration. Obesity is associated with a reduction of BAT function; however, it is unknown how obesity promotes dysfunctional BAT. Here, using a murine model of diet-induced obesity, we determined that obesity causes capillary rarefaction and functional hypoxia in BAT, leading to a BAT "whitening" phenotype that is characterized by mitochondrial dysfunction, lipid droplet accumulation, and decreased expression of *Vegfa*. Targeted deletion of *Vegfa* in adipose tissue of nonobese mice resulted in BAT whitening, supporting a role for decreased vascularity in obesity-associated BAT. Conversely, introduction of VEGF-A specifically into BAT of obese mice restored vascularity, ameliorated brown adipocyte dysfunction, and improved insulin sensitivity. The capillary rarefaction in BAT that was brought about by obesity or *Vegfa* ablation diminished β-adrenergic signaling, increased mitochondrial ROS production, and promoted mitophagy. These data indicate that overnutrition leads to the development of a hypoxic state in BAT, causing it to whiten through mitochondrial dysfunction and loss. Furthermore, these results link obesity-associated BAT whitening to impaired systemic glucose metabolism.

Introduction

Brown adipose tissue (BAT) is activated by the sympathetic nervous system (SNS) to generate heat rather than ATP through uncoupled oxidative phosphorylation (1). BAT is abundant in small rodents and newborn humans and was once thought to disappear in human adulthood. Recent studies, however, have shown that human adults also possess active BAT (2–4). In addition to its thermogenic function, it has been suggested that BAT contributes to systemic metabolism because of its high oxidative capacity (5–7). Because BAT decreases with obesity and aging (4, 8), the decline in BAT function may be linked to impaired metabolism under these conditions. While it has been shown that increasing BAT mass through transplantation improves metabolism parameters in a model of diet-induced obesity (9), most studies on BAT are associative and the molecular mechanisms that contribute to obesity-linked BAT dysfunction are largely unknown.

Recently, a number of studies have pointed to the importance of the microvasculature in controlling adipose tissue inflammation and overall metabolic function (10–12). Studies with obese patients and mice have documented that the white adipose tissues (WAT) of these organisms display capillary rarefaction and evidence of hypoxia, which correlate with inflammatory macrophage infiltration and inflammatory cytokine expression (13–17). WAT levels of VEGF-A, a major proangiogenic cytokine, have been reported to be either decreased (14, 18, 19), increased (16, 20), or unchanged (21) in obesity. However, there is a general consensus that WAT expansion is associated with an insufficient angiogenic response to hypoxia. Whereas a number of studies report that HIF1α is upregulated in WAT in response to obesity (15–17, 19, 20), overexpression of HIF1α fails to produce a proangiogenic response in WAT (19). Furthermore, the chronic overexpression of VEGF-A in

adipose tissue has been shown to have both protective and detrimental effects on metabolic function (10, 12). Likewise, the ablation of the adipose tissue vasculature has been reported to produce both positive and negative effects on systemic metabolism (11, 22).

Compared with WAT, BAT is more extensively vascularized, and VEGF-A–dependent angiogenesis has been shown to be important for the thermogenic response to prolonged cold adaptation (23). However, the role of BAT vascularity in maintaining systemic metabolic homeostasis under conditions of metabolic stress is unknown. Here, we show that obesity causes capillary rarefaction and hypoxia in BAT that is much more robust than in WAT. This condition leads to BAT "whitening" that is associated with diminished β-adrenergic signaling, the accumulation of large lipid droplets, and mitochondrial dysfunction and loss. These changes in the BAT microenvironment impair thermogenic responses and contribute to dysfunctional glucose metabolism.

Results

To assess the role of BAT vascularity in systemic metabolic dysfunction, a model of diet-induced obesity was established by imposing a high-fat, high-sucrose (HFHS) diet on mice for 8 weeks. Compared with normal chow (NC), HFHS diet in mice significantly increased body weight and induced systemic insulin resistance (Supplemental Figure 1, A and B; supplemental material available online with this article; doi:10.1172/JCI71643DS1). Under these conditions, total BAT weight increased (Supplemental Figure 1C) in association with the accumulation of enlarged lipid droplets in BAT cells (Figure 1, A and B) and a 51% reduction in mitochondrial content per cell (Figure 1B), giving the appearance of BAT "whitening." Since BAT consumes lipids stored in cytosol to generate heat through uncoupled respiration, these morphological changes led us to hypothesize that obesity induces BAT to whiten via mitochondrial dysfunction and loss. Consistent with this concept, the expression of the mitochondrial gene *ND5* was reduced
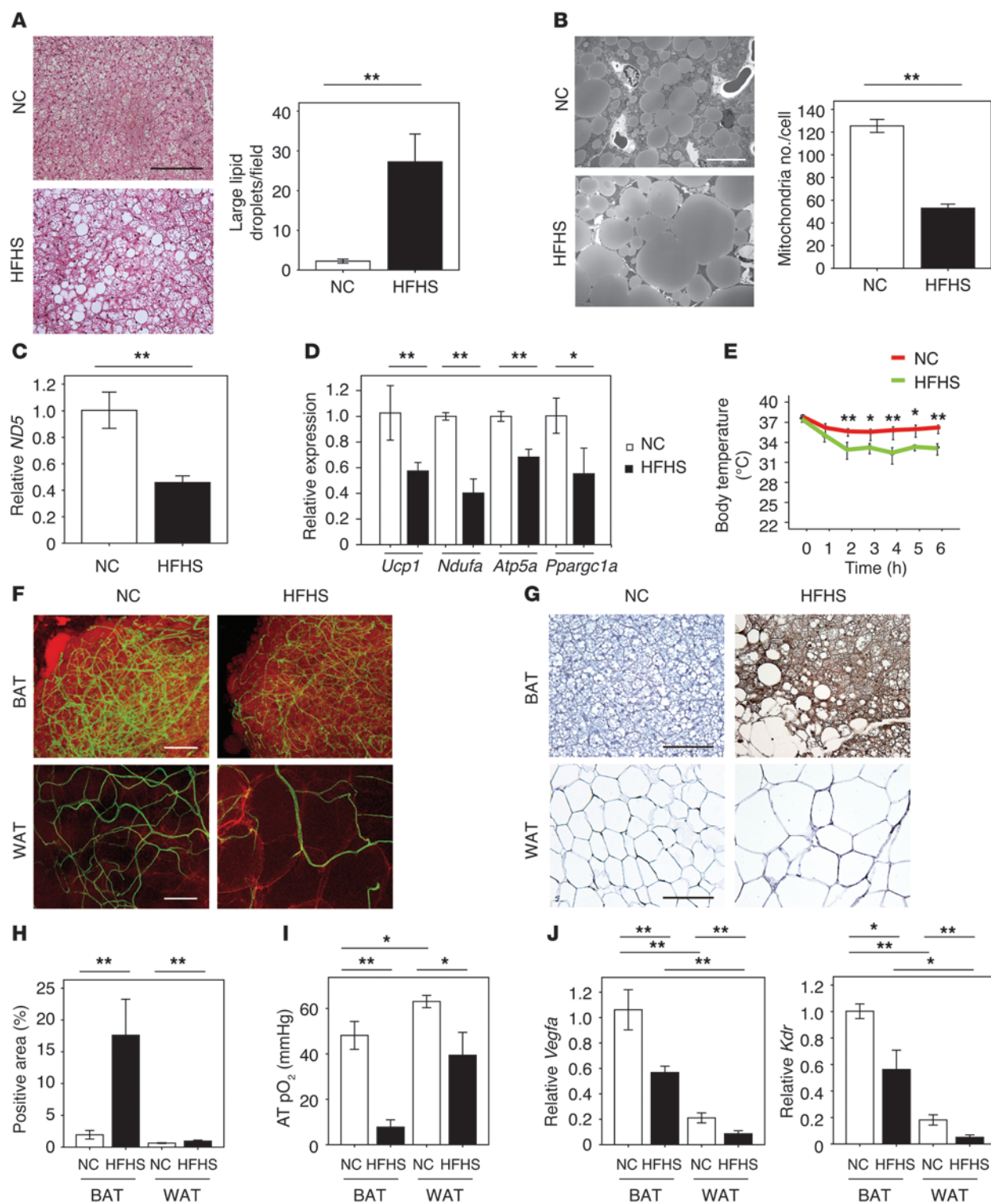
Figure 1

The whitening of BAT associated with capillary rarefaction in diet-induced obesity. (**A**) H&E staining of BAT from mice fed NC or HFHS diet. Scale bar: 50 μm. Right graph shows the number of large lipid droplets/field in BAT (×400, $n = 4$). (**B**) Electron micrographs of BAT from mice fed NC or HFHS diet. Right graph shows the number of mitochondria/cell ($n = 3$). Scale bar: 10 μm. (**C** and **D**) Real-time PCR expression of the mitochondrial-encoded transcript *ND5* and the nucleus-encoded transcripts *Ucp1*, *Ndufa*, *Atp5a*, and *Ppargc1a* in BAT from mice fed NC or HFHS diet ($n = 3$–6). (**E**) Acute CTT for mice fed NC or HFHS ($n = 5$–7). (**F**) Immunofluorescent staining to detect blood vessels with Fluorescein Griffonia (Bandeiraea) Simplicifolia Lectin I (green) and adipocytes with Bodipy-TR (red) in BAT and WAT from mice fed NC or HFHS diet. Scale bars: 100 μm. (**G** and **H**) Pimonidazole staining (**G**) and positive area (**H**) in BAT and WAT of mice fed NC or HFHS diet determined by hypoxyprobe-1 staining ($n = 4$–6). Scale bars: 50 μm. (**I**) Oxygen levels in adipose tissues (AT pO₂ [mmHg]) ($n = 5$–6). (**J**) Real-time PCR expression of *Vegfa* and *Kdr* in BAT and WAT of mice fed NC or HFHS diet ($n = 4$–10). Data were analyzed by 2-tailed Student's *t* test (**A–D** and **H**) or ANOVA (**E**, **I**, and **J**). *$P < 0.05$; **$P < 0.01$. All values represent the mean ± SEM.

(Figure 1C), as was the expression of nuclear-encoded mitochondria marker genes including *Ucp1*, *Ndufa*, *AtpSa*, and *Ppargc1a* relative to β-*actin* expression (Figure 1D). Accordingly, these changes were associated with an impaired thermogenic response in an acute cold–tolerance test (Figure 1E).

Diet-induced obesity led to marked reductions in the vascular network of both BAT and WAT (Figure 1F). An analysis of isolectin IB4–positive vascular structures in tissue sections revealed large reductions in capillary density per unit area and smaller, but statistically significant, reductions in vessel number per adipocyte in both fat depots (Supplemental Figure 1D). However, severe hypoxia, indicated by staining with pimonidazole, was predominantly observed in BAT (Figure 1, G and H). Pimonidazole labeling was also detected in WAT, but the magnitude of the labeling in BAT was much greater. Consistent with these observations, tissue oxygen levels declined markedly in BAT but modestly in WAT in response to dietary obesity, as determined by the measure of oxygen content using a fiber optic oxygen sensor (Figure 1I).

Previous studies have shown that VEGF-A has a crucial role in controlling vascular network formation in adult tissues including WAT and BAT (11, 23). *Vegfa* mRNA was expressed at substantially higher levels in BAT than in WAT (Figure 1J), consistent with the observation that BAT is more highly vascularized than WAT. Under the conditions of these assays, diet-induced obesity was associated with declines in VEGF-A transcript and protein expression in both adipose tissue depots (Figure 1J and Supplemental Figure 1, E–H). Transcript levels of the VEGF-A receptor *Kdr* also declined in parallel with tissue VEGF-A levels, consistent with the reductions in adipose tissue vascularity (Figure 1J).

To explore the temporal relationship between reduced BAT vascularity and markers of mitochondrial dysfunction, WT mice fed a HFHS diet for shorter periods of time (1 and 4 weeks) were analyzed. Relative to mice fed NC, body weight and BAT weight were significantly elevated after 4 weeks on a HFHS diet, but not at 1 week (Supplemental Figure 2A). Correspondingly, lipid droplet enlargement was detected at 4 weeks, but not at 1 week (Supplemental Figure 2B). In contrast, reductions in VEGF-A protein and mRNA expression in BAT could be detected both at 1 and 4 weeks on the HFHS diet, and this corresponded to reductions in the transcript

levels of *Kdr* and to a decrease in capillary density (Supplemental Figure 2, C–E). Staining for pimonidazole indicated the development of robust tissue hypoxia after 4 weeks of HFHS diet (Supplemental Figure 2F). Mitochondrial markers that were reduced by 8 weeks in the BAT of HFHS-fed mice (Figure 1, C and D) were not affected at 1 week. However, *ND5*, *Ndufa*, *Atp5a*, and *Ppargc1a* were downregulated at 4 weeks (Supplemental Figure 2G). These results suggest that capillary rarefaction precedes mitochondrial dysfunction in BAT.

To corroborate these findings, the *ob/ob* genetic model of obesity was examined. As expected, body weight and BAT weight were significantly increased in *ob/ob* relative to control mice (Supplemental Figure 3A), and these changes were associated with the development of the whitening phenotype in BAT and the appearance of enlarged lipid droplets (Supplemental Figure 3B). These changes were associated with marked capillary rarefaction and increased pimonidazole staining in BAT, but the WAT of *ob/ob* mice displayed relatively modest changes in these parameters (Supplemental Figure 3, C and D). VEGF-A protein levels were reduced in the BAT and WAT of *ob/ob* mice (Supplemental Figure 3, E and F), but transcript analyses revealed that *Vegfa* levels were considerably higher in BAT than WAT in the different experimental groups of mice (Supplemental Figure 3G). Transcript analyses also revealed that levels of the vascularity marker *Kdr* were elevated in BAT compared with WAT, and that these levels were reduced in the BAT and WAT of *ob/ob* mice relative to WT (Supplemental Figure 3G). The mitochondrial markers *Ucp1*, *ND5*, *Ndufa*, *Atp5a*, and *Ppargc1a* were also suppressed in the BAT of *ob/ob* mice, and these mice displayed a reduced thermogenic response in an acute cold–tolerance test (Supplemental Figure 3, H and I). These results further indicate that capillary rarefaction and reduced VEGF-A expression are associated with the development of the whitening phenotype in BAT.

VEGF-A ablation leads to BAT whitening. To test whether diminished BAT vascularity is causal for BAT whitening, we generated homozygous adipose tissue–specific *Vegfa*-KO (adipo–*Vegfa*-KO) mice by crossing *Vegfa*flox/flox with *aP2-Cre*+/− mice. No changes in body weight and food intake were observed between the KO mice and WT fed a standard chow diet (Supplemental Figure 4, A and B). The aP2-Cre recombinase activity is expressed in adipose tissues as well as in the central nervous system and macrophages (24, 25); however, there were no significant changes in *Vegfa* expression in bone marrow–derived macrophages, cerebrum, and cerebellum in the *aP2-Cre*+/− *Vegfa*flox/flox mice (data not shown). The genetic disruption of *Vegfa* by aP2-cre significantly reduced VEGF-A transcript and protein levels, by 48% and 63%, respectively, in BAT, and by 32% and 58%, respectively in WAT (Figure 2A and Supplemental Figure 4, C–F), approximately matching the declines in VEGF-A protein expression that are observed in the diet-induced obesity model (Supplemental Figure 1, E–H). Declines in both BAT and WAT vascularity were notable under these conditions (Figure 2B). Analysis of capillary density by immunostaining for isolectin IB4–positive endothelial cells in histological sections revealed a 42% reduction in BAT and a 51% reduction in WAT (Supplemental Figure 4G), which was similar to the declines in vascularity observed in the model of diet-induced obesity (Supplemental Figure 1D). Although *Vegfa* ablation led to a relatively small but detectable pimonidazole reactivity in WAT, the degree of hypoxyprobe signal in BAT was considerably greater (Figure 2C and Supplemental Figure 4H).
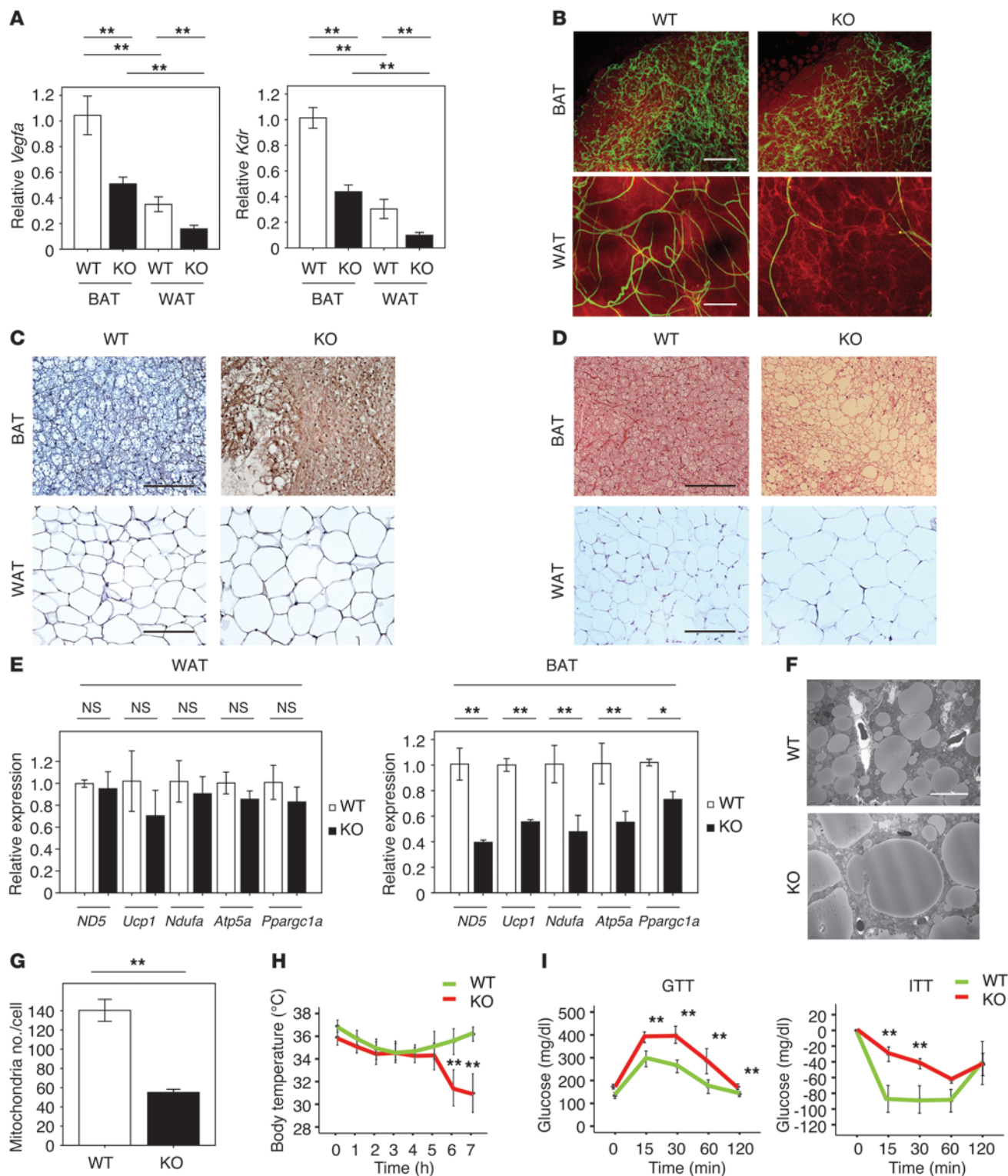
Figure 2

The whitening of BAT and impaired glucose metabolism in aP2-Cre^{+/−} Vegfa[flox/flox] mice. (**A**) Real-time PCR expression of Vegfa and Kdr in BAT and WAT of aP2-Cre^{+/−} Vegfa[flox/flox] (KO) and control Vegfa[flox/flox] mice (WT) (n = 4–19). (**B**) Immunofluorescent staining to detect vasculature with Fluorescein Griffonia (Bandeiraea) Simplicifolia Lectin I (green) and adipocytes with Bodipy-TR (red) in BAT and WAT from WT and KO mice. Scale bars: 100 μm. (**C**) Pimonidazole staining of BAT and WAT from WT and KO mice was performed by the hypoxyprobe-1 method. Scale bars: 50 μm. (**D**) H&E staining of BAT and WAT from WT and KO mice. Scale bars: 50 μm. (**E**) Real-time PCR detecting expression of ND5, Ucp1, Ndufa, Atp5a, and Ppargc1a in WAT and BAT of WT and KO mice (n = 3–6). (**F** and **G**) Electron micrographs of BAT of WT and KO mice (**F**) and the number of mitochondria/cell (**G**) (n = 3). Scale bar: 10 μm. (**H**) Acute CTT for mice prepared in **A** (n = 7). (**I**) GTT and ITT of mice prepared in **A** (n = 5–7). Data were analyzed by 2-tailed Student's t test (**E** and **G**) or ANOVA (**A**, **H**, and **I**). *$P < 0.05$; **$P < 0.01$. All values represent the mean ± SEM.

An analysis of WAT revealed that Vegfa ablation led to an enlargement in average cell size and a modest increase in total tissue weight (Figure 2D and Supplemental Figure 4, I and J), although a statistically significant change in overall body weight was not observed. However, Vegfa ablation produced little or no changes in expression of inflammatory markers that contribute to systemic insulin resistance, such as EGF-like module-containing mucin-like hormone receptor-like 1 (Emr1), TNF-α, and chemokine (C-C motif) ligand 2 (Ccl2/MCP-1) (data not shown), nor were there detectable changes in the expression of mitochondrial markers including ND5, Ucp1, Ndufa, Atp5a, and Ppargc1a in WAT (Figure 2E). In marked contrast to effects on WAT, Vegfa ablation led to a significant reduction in BAT mass (Supplemental Figure 4, K and L). Histological analysis of BAT revealed that VEGF-A deficiency led to a whitening phenotype that was accompanied by an increase in lipid droplet size and a reduction in mitochondrial number within BAT adipocytes (Figure 2, D, F, and G, and Supplemental Figure 4M). In contrast to WAT, the transcript expression levels of mitochondrial marker proteins were suppressed in BAT by adipose tissue Vegfa ablation (Figure 2E). These changes were associated with an impaired thermogenic response (Figure 2H), consistent with results of systemic Vegfr2 blockade (23). Vegfa ablation also led to modest impairment in glucose metabolism in mice fed the NC diet (Figure 2I). Collectively, these data suggest that the BAT phenotype resulting from Vegfa ablation is similar to that seen in conditions of diet-induced obesity in WT mice. These findings led us to hypothesize that capillary rarefaction in adipose tissue can lead to the selective development of a hypoxic state in BAT that promotes BAT dysfunction.

BAT-specific VEGF-A rescue improves BAT function and systemic glucose metabolism. To assess the functional significance of BAT hypoxia in obese or Adipo-Vegfa-KO mouse models, we performed gain-of-function experiments by injecting an adenoviral vector encoding Vegfa (ad-vegfa), or a control vector expressing β-gal directly into interscapular BAT (Supplemental Figure 5A). Transduction with a low dose of vector led to a doubling of VEGF-A transcript and protein levels in the BAT of NC-fed mice at 1 week after delivery, whereas the level of VEGF-A achieved in BAT of HFHS-fed mice approximately matched that of the control, NC-fed conditions (Figure 3A and Supplemental Figure 5B). Ad-vegfa delivery to BAT did not affect Vegfa or Kdr levels in epididymal WAT (Figure 3B). However, restoration of VEGF-A in the BAT of HFHS-fed mice

reversed the decline in vascular density that was caused by dietary obesity as assessed by measures of vessel density and Kdr expression (Figure 3, A and C, and Supplemental Figure 5, C and D). Vegfa transduction of the BAT of obese mice suppressed the development of enlarged lipid droplets, and this was associated with the upregulation of ND5, Ucp1, Ndufa, and Ppargc1a transcripts that encode for mitochondria-associated proteins (Figure 3, D–F). Vegfa transduction of BAT normalized the thermogenic response to acute cold exposure in obese mice (Figure 3G). Vegfa delivery to the BAT also increased glucose uptake by BAT and improved systemic insulin sensitivity in obese mice (Figure 3, H and I).

At this low dose of Ad-Vegfa vector, vessel leakage in BAT was not detected following the injection of FITC-dextran (Supplemental Figure 6A), and there was no increase in markers of adipose tissue inflammation when the Ad-Vegfa vector was administered to the BAT of NC-fed mice (Supplemental Figure 6B). There were no detectable increase in serum VEGF-A levels determined by ELISA (Supplemental Figure 6C) and no detectable transgene expression or changes in vessel density in WAT (Supplemental Figure 6, D–F) or liver (data not shown). Ad-vegfa delivery to BAT did not lead to morphological changes in WAT adipocyte size and had no effect on the expression profiles of proinflammatory cytokines in the WAT of mice subjected to either NC or HFHS diets (Supplemental Figure 6, G and H), consistent with the lack of detectable transgene expression in WAT. Furthermore, the adenovirus treatment did not affect WAT weight, body weight, or food intake (Supplemental Figure 6, I–K). Ad-vegfa transduction of the BAT cell line did not change the expression profiles of mitochondria (ND5, Ucp1, Ndufa, Atp5a, Ppargc1a) or mitophagy (LC3 and Bnip3) markers (data not shown), suggesting that VEGF acts on BAT through its ability to restore vascularity. Finally Vegfa delivery to BAT of WT mice fed NC led to the overexpression of VEGF-A and increased BAT vessel density (Figure 3, A and C, and Supplemental Figure 5, B and C), but in contrast to findings in mice fed HFHS, this did not affect mitochondrial marker expression (Figure 3F), thermogenic response to acute cold exposure (Figure 3G), or metabolic responses to glucose or insulin under these conditions (Figure 3I).

Ad-vegfa delivery to BAT was also assessed in adipo–Vegfa-KO and littermate control mice. VEGF-A rescue of the KO mice significantly increased the microvascular density of BAT (Supplemental Figure 7, A–C). Restoration of BAT vasculature promoted the "rebrowning" of BAT in the adipo–Vegfa-KO that was characterized by a reduction in the frequency of large lipid droplets and increased expression of ND5, Ndufa1, and Ppargc1a (Supplemental Figure 7, D and E). These changes were associated with the recovery of the thermogenic response in a cold-tolerance test and improved glucose metabolism in the lean KO mice (Supplemental Figure 7, F and G). However, delivery of Vegfa to BAT of adipo–Vegfa-KO mice had no detectable impact on WAT and body weight (Supplemental Figure 7, H and I) or vascularity in WAT (data not shown), suggesting that recovery of the vasculature in BAT leads to improved systemic metabolic function irrespective of the WAT phenotype.

Hypoxia promotes mitochondrial dysfunction and mitophagy in BAT. Mitochondria generate ROS during hypoxia (26, 27), contributing to mitochondrial damage that upregulates autophagic and apoptotic pathways (28). Thus, we hypothesized that capillary rarefaction in BAT would contribute to mitochondrial dysfunction and loss. Both diet-induced obesity and adipose tissue Vegfa ablation led to significantly elevated superoxide levels in mito-
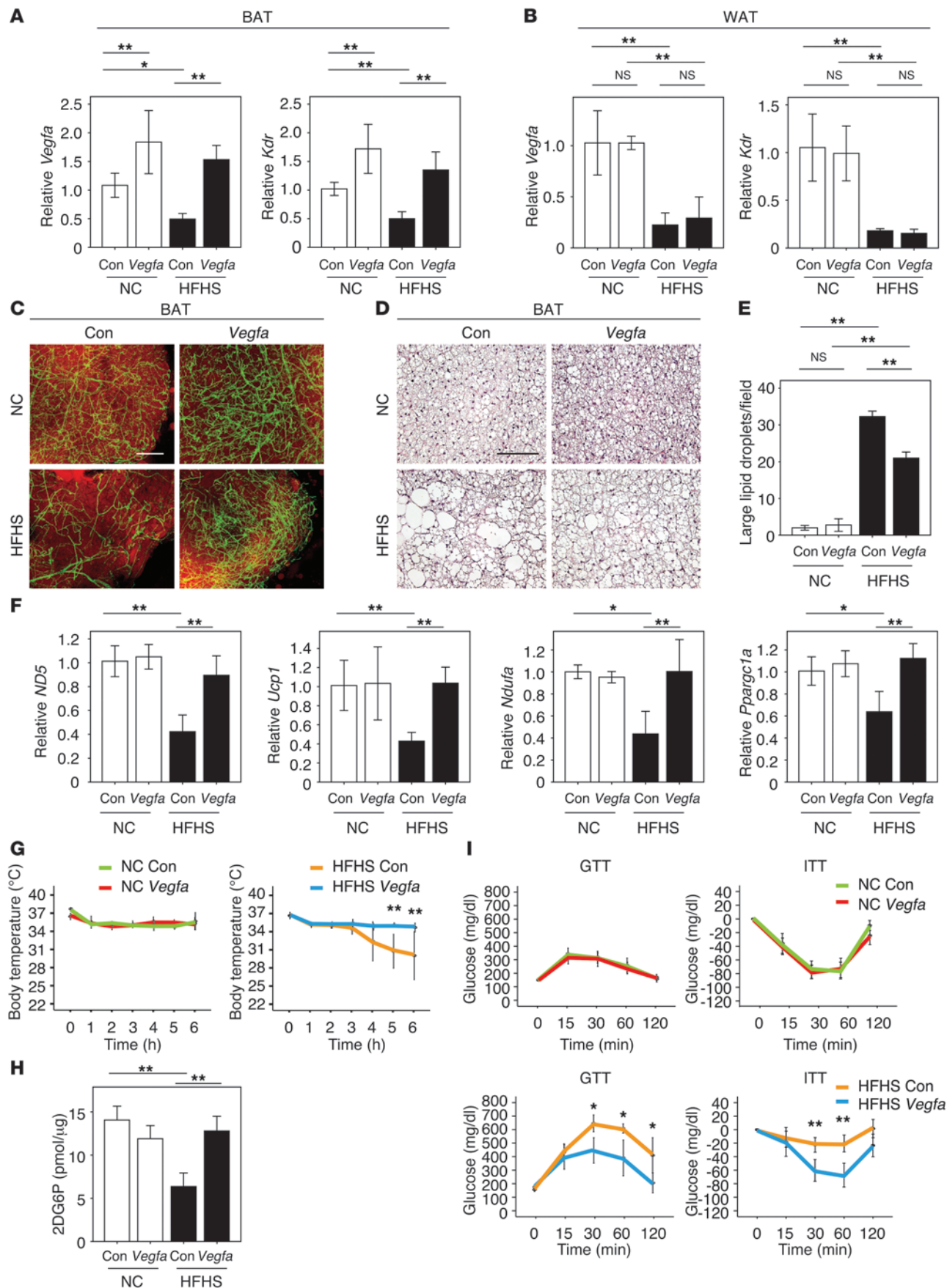
Figure 3

BAT-specific *Vegfa* delivery induces the rebrowning of the whitened BAT in dietary obesity. (**A** and **B**) Real-time PCR analysis of *Vegfa* and *Kdr* expression in BAT (**A**) and WAT (**B**) of mice after injection of ad-*vegfa* or control vector into BAT of mice fed NC or HFHS diets. ad-*lacZ* was used as a control (Con) (n = 5–8). (**C**) Immunofluorescent staining with Fluorescein Griffonia (Bandeiraea) Simplicifolia Lectin I (green) to detect vasculature and with Bodipy-TR (red) to detect lipid in BAT from NC- or HFHS-fed mice after the injection of ad-*vegfa* of the control adenoviral vector. Scale bar: 100 μm. (**D**) H&E staining of BAT from NC- and HFHS-fed mice prepared in **A** after the injection of ad-*vegfa* or a control adenoviral vector. Scale bar: 50 μm. (**E**) Quantitative analysis of the number of large lipid droplets/field in BAT under the different experimental conditions (×400, n = 4). (**F**) Real-time PCR analysis of the expression of *ND5*, *Ucp1*, *Ndufa*, and *Ppargc1a* in BAT of mice described in **A** (n = 3–10). (**G**) Acute CTT of the different experimental groups of mice (n = 3–7). (**H**) Glucose uptake by BAT was evaluated by measuring 2DG uptake (n = 4–6). (**I**) GTT and ITT in the different experimental groups of mice receiving ad-*vegfa* or control adenovirus (n = 4–8). Data were analyzed by ANOVA (**A**, **B**, and **E**–**I**). *P < 0.05; **P < 0.01. All values represent the mean ± SEM.

chondria isolated from BAT, as detected by flow cytometric analysis of MitoSOX staining (Figure 4A and Supplemental Figure 8, A and B). These changes were associated with a downward shift in mitochondrial membrane potential determined by flow cytometric analysis of Mito Red staining (Figure 4B and Supplemental Figure 8, C and D). Treatment with CCCP, an uncoupler of oxidative phosphorylation, led to a near complete collapse of membrane potential in these assays (Figure 4B).

Diet-induced obesity led to a significant increase in the expression of the autophagosomal protein LC3A/B-II in BAT (Figure 4C). Histological analysis of tissue sections revealed that LC3 formed puncta that colocalized with the mitochondrial marker Tom20 (Figure 4D). Similarly, *Vegfa* ablation in BAT led to the coalescence of LC3 into puncta that colocalized with mitochondria (Supplemental Figure 8E). Consistent with these observations, levels of the autophagy markers *Bnip3* and *Map1lc3b* were increased in the BAT of dietary obese and VEGF-A–deficient mice (Figure 4E and Supplemental Figure 8F). The LC3-positive puncta phenotype was reversed by ad-*vegfa* delivery into BAT (Figure 4F and Supplemental Figure 8G), and this treatment also led to reductions in *Bnip3* and *Map1lc3b* expression in both models (Figure 4G and Supplemental Figure 8H). PTEN-induced putative kinase protein 1 (PINK1) promotes mitophagy via the Parkin-dependent ubiquitination of mitochondria (29). Consistent with an increased mitophagic response in the BAT of the dietary obese model, there were significant increases in the expression of both PINK1 and Parkin, and there was a marked increase in the ubiquitination of the mitochondrial proteins (Figure 4, H–J). Collectively, these results suggest that obesity leads to hypoxic stress in BAT, promoting the activation of a mitophagic program via the PINK1-Parkin system.

To test whether hypoxia per se is sufficient to induce mitochondrial dysfunction and autophagy, BAT from WT mice was cultured ex vivo under normoxic and hypoxic conditions. Hypoxia significantly increased mitochondrial ROS production, which was associated with a reduction in mitochondrial membrane potential (Supplemental Figure 9, A and B). This condition also led to increased LC3A/B-II protein expression and elevations in *Bnip3* and *Map1lc3b* levels, whereas the expression levels of mitochondrial marker genes

were reduced (Supplemental Figure 9, C–E). The effects of hypoxia on a brown adipocyte cell line were also evaluated. Hypoxic conditions increased mitochondrial ROS and led to a reduction in mitochondrial membrane potential (Supplemental Figure 9, F–H). Hypoxia led to an upregulation of LC3A/B-II protein expression, and the LC3 signal was associated with mitochondria, indicative of an autophagic response (Supplemental Figure 9, I–K). Hypoxia also promoted *Bnip3* and *Map1lc3b* expression (Supplemental Figure 9L). Conversely, levels of the mitochondrial markers, such as *ND5*, *Ndufa*, and *Ppargc1a*, were reduced under conditions of hypoxia (Supplemental Figure 9M), consistent with mitochondrial dysfunction and loss in the brown adipocyte cell line.

Hypoxic conditions during WAT expansion lead to the induction of Hif1α (13, 15, 16). However, in this context, Hif1α is not proangiogenic and its overexpression fails to induce Vegfa in adipose tissue (19, 30). In our study, dietary obesity led to an increase in Hif1α levels both in BAT and WAT, but the magnitude of the induction was much greater in BAT (Supplemental Figure 10A). Hypoxia also increased Hif1α protein levels in the brown adipocyte cell line (Supplemental Figure 10B). Hif1α is reported to induce autophagy via the induction of Bnip3 (31), but a potential role of Hif1α in mitochondrial clearance in adipose tissues has not been explored previously. Transduction of the cultured brown adipocyte line under normoxic conditions with an adenoviral vector expressing *Hif1a* (ad-*Hif1a*) did not upregulate *Vegfa* expression (Supplemental Figure 10, C and D), but increased *Bnip3* and reduced *ND5* levels (Supplemental Figure 10, E and F), which is consistent with the activation of a mitophagic response. Similarly, the injection of ad-*Hif1a* into the interscapular BAT of mice did not increase *Vegfa* levels (Supplemental Figure 10, G and H). However, delivery of ad-*Hif1a* to BAT increased *Bnip3* expression and reduced *ND5* (Supplemental Figure 10, I and J). Transduction of *Hif1a* into BAT also increased other Hif1a target genes involved in fibrotic processes such as elastin (*Eln*) and lysyl oxidase (*Lox*) (Supplemental Figure 10K); however, other target genes such as *Glut1*, hexokinase-2 (*HK2*) and pyruvate kinase PKM (*Pkm2*) showed no significant change (data not shown). *Eln* and *Lox* expression were also increased in the BAT of dietary obese mice (Supplemental Figure 10L). These results suggest that Hif1α is not proangiogenic in BAT, but that it may be involved in the induction of mitophagy or fibrotic processes triggered by hypoxia.

Hypoxia inhibits β-adrenergic signaling in BAT. β-Adrenergic signaling activates Vegfa expression in BAT via activation of cAMP-dependent PKA (32). Whereas sympathetic overactivity is generally associated with obesity (33), catecholamine sensitivity is decreased in the BAT of obese organisms (34) due at least in part to diminished β-adrenergic receptor expression (35, 36). In the model of diet-induced obesity employed in this study, significant reductions in β1- and β3-adrenergic receptor expression in BAT were observed after imposing the HFHS diet (Figure 5A). BAT hypoxia, imposed by VEGF deficiency, also led to similar reductions in β1- and β3-adrenergic receptor expression in BAT (Figure 5B). Whereas levels of the *Adrb3* transcript were present at a higher copy number than *Adrb1* in BAT, obesity and hypoxia led to a similar reduction in the expression of these receptor transcripts. These changes in receptor expression caused by dietary obesity or genetic *Vegfa* ablation led to accompanying reductions in PKA signaling (Figure 5, C and D). These data suggest that intracellular lipid droplet enlargement (whitening) is due in part to the downregulation in β-adrenergic signaling.
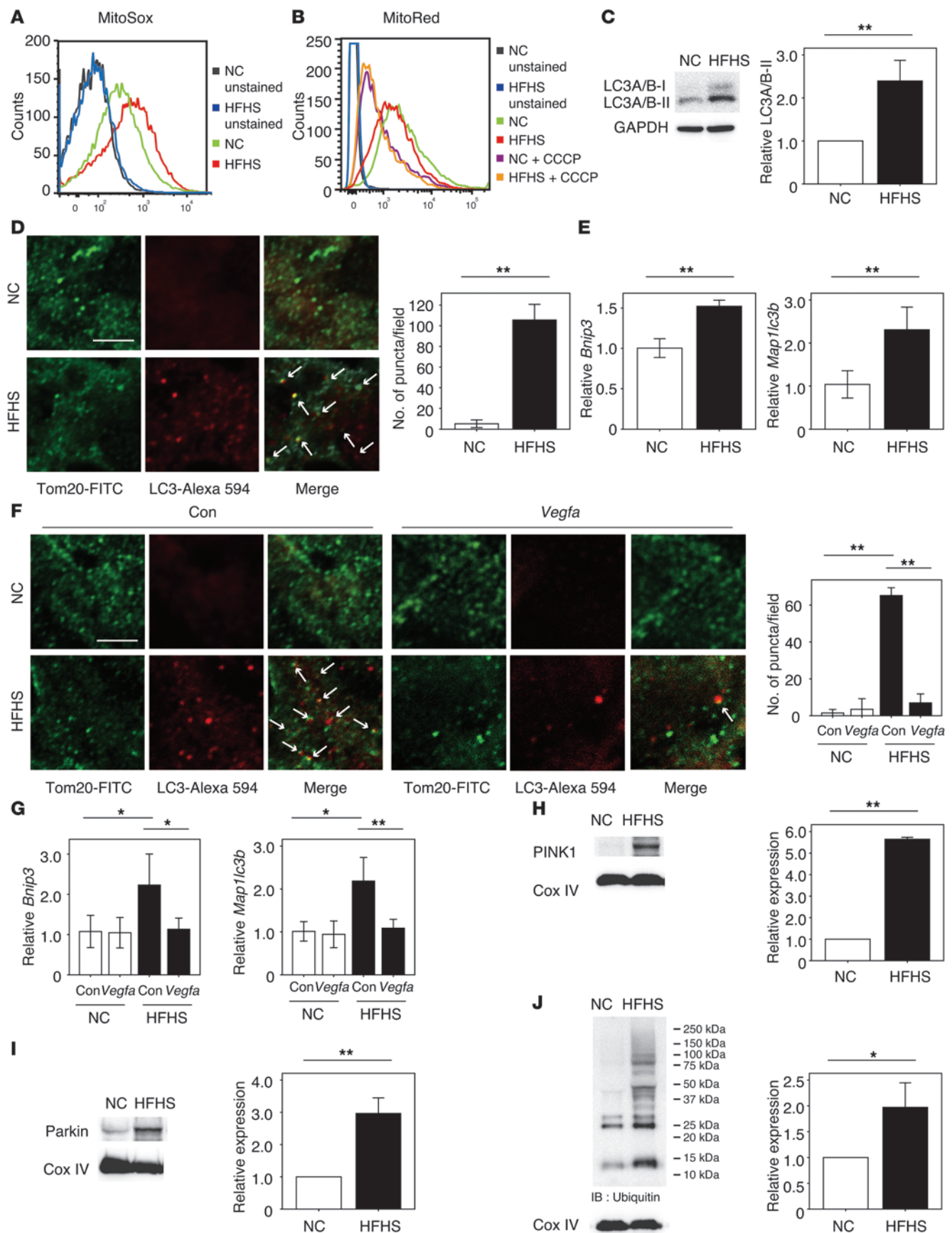
Figure 4

VEGF-A–mediated regulation of mitochondrial ROS production and autophagic responses in the BAT of obese mice. (**A** and **B**) FACS analysis for mitochondrial ROS (MitoSOX; **A**) and membrane potential (MitoRed with or without CCCP treatment; **B**) using isolated mitochondria extracted from BAT. (**C**) Western blot analysis of LC3A/B expression in BAT. The right graph indicates the quantification of LC3A/B-II expression relative to GAPDH-loading control ($n = 3$). (**D** and **F**) Immunofluorescent staining showing mitochondrial membrane protein Tom20 (green) colocalizing with autophagosomal membrane protein LC3 (red) in BAT of mice fed NC or HFHS diet with (**F**) or without (**D**) the injection of ad-*vegfa* or a control adenoviral vector (Con). Representative photomicrograph observed at ×3000 magnification. Scale bar: 3 μm. Merged areas are indicated by white arrows. The graph at right quantifies the number of puncta double stained with Tom20 and LC3 measured on 10 random fields and observed at ×3000 magnification ($n = 3$). (**E** and **G**) Real-time PCR expression of *Bnip3* and *Map1lc3b* in BAT of mice ($n = 3$–6). (**H**–**J**) Western blot analysis of PINK1 (**H**), Parkin (**I**), and ubiquitin-conjugated protein (**J**) expression in isolated mitochondria extracted from BAT of mice. The graphs at right indicate the quantification relative to the expression of the Cox IV loading control ($n = 3$). In **J**, the level of ubiquitination is compared with the 25 kDa protein between the groups. Data were analyzed by 2-tailed Student's *t* test (**C**–**E** and **H**–**J**) or ANOVA (**F** and **G**). *$P < 0.05$; **$P < 0.01$. All values represent the mean ± SEM.

To define aspects of the mechanisms by which metabolic dysfunction contributes to hypoxia-mediated BAT dysfunction, FFA levels were determined in the different experimental groups of mice. As expected, HFHS diet led to elevation in FFA levels in BAT at 8 weeks (Supplemental Figure 11A), and this increase in FFA levels in BAT was detected as early as 1 week after initiating the feeding regimen (Supplemental Figure 11B). In the brown adipocyte cell line, treatment with palmitic acid led to a reduction in VEGF-A protein and transcript expression (Supplemental Figure 11, C and D), as would be expected from its ability to downregulate PKA-targeted gene expression (37). In contrast, palmitic acid did not downregulate *Adrb1* or *Adrb3* expression (Supplemental Figure 11E). However, exposure to hypoxia for 24 hours was sufficient to downregulate receptor expression in the brown adipocyte cell line (Supplemental Figure 11, F and G), and this corresponded to reductions in receptor density (Supplemental Figure 11, H and I), PKA phosphorylation (Supplemental Figure 11J), and cAMP levels (Supplemental Figure 11K). Since it is established that VEGF is regulated by β-adrenergic signaling in BAT (32, 38, 39), these data suggest that multiple regulatory inputs contribute to the downregulation of VEGF in BAT under conditions of obesity (Figure 5E).

Discussion

Here, we delineate the molecular mechanisms that contribute to BAT dysfunction under conditions of obesity. BAT dysfunction, which led to an impaired response to an acute cold challenge, was associated with the accumulation of enlarged lipid droplets and with the loss of mitochondria, giving the tissue a whitened phenotype. BAT whitening corresponded to the reduced expression of mitochondria-associated transcripts, including *ND5*, *Ucp1*, and *Ppargc1a*, elevated mitochondrial ROS production, and membrane depolarization. BAT whitening also corresponded to an increase in mitophagy, as indicated by the appearance of LC3 puncta with mitochondria, increased localization of the mitophagy proteins PINK1 and Parkin to mitochondria, and an increased level of mitochondrial protein ubiquitination.

A number of lines of evidence suggest that the mechanism of obesity-mediated mitochondrial loss and BAT dysfunction is due in part to capillary rarefaction. First, the reduction in capillarization and VEGF expression in BAT precedes the loss of mitochondrial marker gene expression and the appearance of the whitened BAT phenotype during the development of diet-induced obesity. Furthermore, the targeted ablation of *Vegfa* using aP2-Cre decreased VEGF-A levels and capillary density within BAT to levels that are similar in magnitude to those observed in diet-induced obesity. This genetic manipulation produced a phenotype in BAT of mice fed NC that has features in common with dietary obesity, including impaired thermogenic function and tissue whitening. Under these conditions, mitochondrial dysfunction in BAT was characterized by lipid droplet accumulation, elevated mitochondrial ROS production, decreased mitochondrial membrane potential, and increased mitophagy.

Causal evidence for a functional role of vascular rarefaction in BAT dysfunction was provided by rescue experiments in which specific VEGF-A–mediated revascularization of BAT resulted in rebrowning of the tissue and normalization of the phenotype. In both models of dietary obesity and adipose tissue *Vegfa* ablation, BAT revascularization led to a reduction in lipid droplet accumulation, restored mitochondrial function, and diminished mitophagy and improved the thermogenic response to cold challenge. Notably, BAT revascularization also led to an improvement in insulin resistance, consistent with the notion that this tissue contributes to whole-body glucose metabolism in mice (5, 9). These data indicate that changes in the BAT microenvironment, in particular the status of its vascular network, can significantly affect systemic metabolic function in mice.

Mechanistic studies reveal that both obesity and VEGF ablation lead to the downregulation of β-adrenergic signaling in BAT. It is widely recognized that VEGF expression in BAT is under the control of the SNS (32, 38, 39). As shown here, diet-induced obesity led to marked reductions in the expression of the β1- and β3-adrenergic receptors, with an accompanying decrease in PKA signaling. In part, this regulation can be attributed to an increase in the level of FFA, and we show that palmitic acid can downregulate VEGF expression in the cultured brown adipocyte line. However, palmitic acid did not downregulate β-adrenergic receptor expression, consistent with the finding that fatty acids act at the level of adenylate cyclase activity to interfere with β-adrenergic signaling (37). In contrast, hypoxia will lead to marked reductions of β1- and β3-adrenergic receptor expression in cultured brown adipocytes. Furthermore, adipose tissue hypoxia, induced by VEGF ablation, was sufficient to downregulate β-adrenergic receptor expression and signaling in vivo. These data, combined with the observation that diminished VEGF expression and capillarization precede the decline in adrenergic receptor expression in diet-induced obesity, suggest that hypoxia is a key regulatory feature in the inhibition of β-adrenergic signaling and the whitening of BAT. These data also suggest the existence of a pathological feedback loop in which diminished β-adrenergic signaling in BAT leads to reductions in VEGF and capillarization under conditions of obesity. In turn, the development of a hypoxic state in BAT further impairs β-adrenergic signaling in this tissue (Figure 5E).

Prior studies have shown that experimental and clinical obesity are associated with moderate reductions in VEGF-A levels and capillary rarefaction in WAT (14, 40, 41). These findings have led to the concept that declines in WAT perfusion can exacerbate
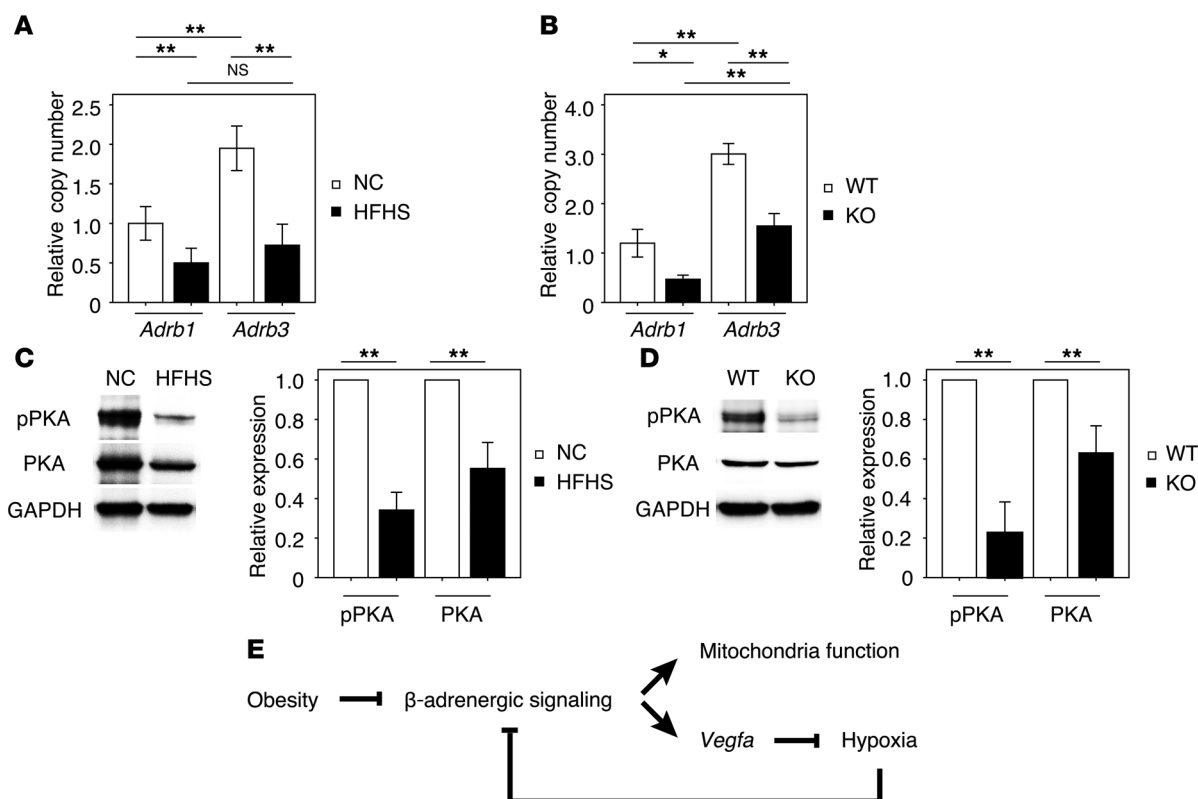
Figure 5
Hypoxia inhibits β-adrenergic signaling. (**A**) Relative copy number of *Adrb1* and *Adrb3* transcript expression in BAT under these experimental conditions (*n* = 4–5). (**B**) Relative copy number of *Adrb1* and *Adrb3* transcript expression in BAT of the KO and WT mice (*n* = 3–8). (**C** and **D**) Western blot analysis of phosphorylated PKA (pPKA Thr197) and total PKA in BAT from mice fed NC or HFHS diet or BAT from *aP2-Cre*^{+/–} *Vegfa*[flox/flox] (KO) and control *Vegfa*[flox/flox] mice (WT). Right graphs indicate quantification relative to PKA (for pPKA) and GAPDH-loading control (for PKA) (*n* = 3). (**E**) Graphical illustration of the downregulation of adrenergic signaling under conditions of obesity and the proposed positive feedback loop caused by hypoxic conditions. Data were analyzed by 2-tailed Student's *t* test (**C** and **D**) or ANOVA (**A** and **B**). *$P < 0.05$; **$P < 0.01$. All values represent the mean ± SEM.

insulin resistance due to hypoxic stresses, leading to adipose tissue inflammation. Most data in support of this hypothesis are associative, and causal data linking vascular rarefaction in fat with metabolic dysfunction has been lacking. To assess whether impairments in perfusion are responsible for triggering the dysfunctional phenotype in fat, studies have sought to examine the consequences of either promoting or ablating the vasculature in adipose tissue (10–12, 22, 42–44). Findings from these studies appear to be contradictory, suggesting that the control of the adipose tissue function by the vascular microenvironment is complex and, perhaps, dependent upon the temporal stage of obesity (reviewed in ref. 45). Notably, these studies have primarily focused on the role of the vasculature in WAT, while BAT has typically received a cursory histological examination. The results from our study suggest that physiologically relevant perturbations in VEGF-A levels and vascular density can markedly alter BAT function, yet have limited effects on WAT. Evidence for a far greater extent of hypoxia in BAT than WAT in obese mice includes greater reactivity with the pimidazole stain, higher HIF1α expression, and reduced interstitial oxygen content determined with a fiber optic oxygen microsensor. VEGF-A levels and vascular density are approximately 5- to 10-fold higher in BAT than WAT, yet the percentage declines in these parameters resulting from diet-

induced obesity are similar between these 2 depots. Ablation of *Vegfa* in aP2-Cre–expressing cells resulted in changes that approximately matched declines in VEGF-A and capillary rarefaction seen in dietary obesity in both WAT and BAT. However, diminished VEGF-A expression, via gene ablation, produced relatively modest or no evidence of WAT dysfunction as assessed by measures of hypoxia, inflammation, and mitochondrial marker expression. Similarly, recent analyses of human WAT do not find evidence for a hypoxic state in obesity (40, 46). In contrast, robust BAT dysfunction in mice was evident based upon a multitude of molecular and physiological measurements. The disparate responses of WAT and BAT to reductions in VEGF-A are consistent with the greater respiratory capacity in BAT than WAT, owing to the fact that BAT primarily functions to consume energy and dissipate heat whereas WAT primarily functions to store energy. Furthermore, WAT has a higher lipid content than BAT, and O_2, being nonpolar, is more soluble in the hydrophobic environment of the WAT versus the BAT adipocyte, facilitating its diffusion (47).

Several lines of evidence have shown that autophagy has pivotal roles in the regulation of metabolism. Autophagy is activated under conditions of stress including starvation, ischemia-reperfusion, pathogen infection, ROS stress, and hypoxia (48). A basal level of autophagy is generally considered to have a crucial

role in removing and renewing dysfunctional mitochondria and maintaining homeostasis. However, autophagy is reported to have both protective and detrimental roles in metabolic disorders. A decrease in hepatic autophagy was observed in a murine model of diet-induced obesity, and restoration of the autophagic response in the liver improves systemic glucose metabolism by enhancing hepatic insulin action (49). In contrast, the forced downregulation of autophagy in adipose tissue was shown to improve insulin sensitivity in obese mice (50, 51). In these studies, the attenuation of autophagy in adipose tissue was associated with the acquisition of BAT characteristics by WAT, such as an increase in mitochondrial number and greater fatty acid β-oxidation. These results are consistent with the findings of our study, in which an elevated level of mitochondrial autophagy was detected in the BAT of mice subjected to high-calorie diet or adipose tissue *Vegfa* ablation. It is well established that hypoxic stress promotes ROS production by dysfunctional mitochondria (52). In turn, the elimination of dysfunctional mitochondria through autophagy is a mechanism to limit toxic levels of ROS (53). Therefore, we speculate that the upregulation of mitophagy in BAT is a compensatory response to the ischemic stress that is imposed on mitochondria by overnutrition. In other words, BAT acquires WAT characteristics under conditions of dietary obesity because vascular rarefaction drives the mitochondrial dysfunction and elimination, shifting the equilibrium toward lipid storage.

Studies have analyzed the "browning" of WAT as a strategy for combating obesity (54–56). However, it has been argued that these actions are quantitatively incapable of significantly affecting systemic metabolism due to the low thermogenic capacity of WAT browning relative to that exhibited by classical BAT depots (57). Comparatively little attention has been given to the mechanisms that contribute to BAT dysfunction and how they affect overall metabolic health. As shown here, the status of the vasculature in BAT is critical for its function both in terms of thermogenesis and systemic metabolic homeostasis. Thus, risk factors that are associated with diminished vascular health, such as hypertension, hypercholesterolemia, and physical inactivity, could contribute to the development of obesity through the degradation of BAT function.

Methods

Animal models. All mice were on a C57BL/6 background, and 4-week-old WT male mice were purchased from Charles River Laboratories. These mice were maintained on a HFHS diet (number F1850; Bio-Serv) for 8 weeks, starting at 4 weeks of age. In some experiments, mice were fed a HFHS diet for 1 or 4 weeks, starting at 4 weeks of age. The composition of the HFHS diet was 35.8% fat (primarily lard), 36.8% carbohydrate (primarily sucrose), and 20.3% protein. Analysis was done at 12 to 14 weeks of age. aP2-Cre (Jackson Laboratories) and *Vegfa^flox/flox* mice (provided by Napoleone Ferrara, Genentech Inc.) on a C57BL/6 background were crossed to create *aP2-Cre^+/– Vegfa^flox/flox* adipose tissue–specific *Vegfa*-KO mice. *Vegfa^flox/flox* mice were used as a control. The genotyping for these mice was conducted as previously described (58). Glucose uptake measurements of BAT were performed with the 2DG Uptake Measurement Kit (COSMO BIO Co., LTD) according to the manufacturer's instructions. Mice fed with an NC or a HFHS diet for 8 weeks were fasted for 4 hours, and 5 μmol 2-deoxyglucose (2DG) was injected via tail vein. After 20 minutes, BAT was collected for further analysis.

Adenovirus. Full-length mouse *Vegfa_164* cDNA was subcloned into an adenovirus shuttle vector to generate the recombinant adenoviral vector expressing *Vegfa_164* (ad-*vegfa*) according to the manufacturer's instructions (AdEasy system; Agilent Technologies). An adenoviral vector expressing *lacZ* (ad-*lacZ*) was used as a control. Adenoviral vectors were purified by Adeno-X Maxi Purification Kit (Clontech Laboratories). Mice were fixed in prone posture. Constant anesthesia was obtained with persistent treatment with isoflurane through a nasal cannula. An incision of approximately 7 mm was made in the posterior region of the neck, which enabled direct visualization of BAT. Adenovirus diluted in 50 μl PBS was injected directly into the left and right lobes of the BAT through a 30G syringe. The titer of adenovirus was 5.0×10^8 PFU/body. Ten-week-old mice were treated with ad-*vegfa* or ad-*Hif1a* injection, and physiological studies were performed at postoperative days 14 to 21. Mice were sacrificed for further analysis at postoperative days 22 to 24 unless otherwise mentioned. Ad-*Hif1a* was purchased from Vector Biolabs.

Systemic metabolic parameters. Mice were individually housed for 1 week prior to starting the assay. On the day of glucose tolerance testing (GTT), mice were fasted for 6 hours, then given glucose i.p. at a dose of 2 g/kg body weight in the early afternoon. For the insulin tolerance test (ITT), mice given human insulin i.p. (1 U/kg body weight) at 1:00 pm without fasting. Blood glucose levels were measured with a glucose analyzer (Roche Diagnostics) at 15, 30, 60, 120 minutes after glucose or insulin injection. All the experiments except for adenovirus treatment were performed at 12 weeks of age.

Acute cold exposure. Body temperature was assessed by the subcutaneous implantation of biocompatible and sterile microchip transponders (IPTT-300 Extended Accuracy Calibration; Bio Medic Data Systems) over the shoulder blades as instructed by the manufacturer. Animals were subjected to cold tolerance test (CTT), and body temperature was measured every hour for 6 to 7 hours. All the experiments except for adenovirus treatment were performed at 12 weeks of age.

Histology. A portion of the BAT and WAT fat pad were fixed in 10% formalin and embedded in paraffin. General morphology was evaluated with H&E staining. Large lipid droplets were defined as lipids larger than 50 μm², measured with ImageJ, and counted per field at ×400 magnification. Ten fields were randomly selected from each sample (*n* = 4 mice per experimental group). Electron microscopy was performed using JEOL 2010 TEM, located at Biology Core, Boston University Medical Campus. Forty cells were randomly selected per group, and intracellular mitochondria were counted. Vascularity was evaluated by staining for isolectin IB4 conjugates (Invitrogen), and vessel number was counted per field at ×400 magnification. Ten fields were randomly selected from each sample (*n* = 4 mice per experimental group) for 4 samples. Protein levels of VEGF-A were evaluated by staining for VEGF (A-20) (Santa Cruz Biotechnology Inc.), and VEGF-A–positive area were measured per field at ×630 magnification for BAT and ×200 magnification for WAT. Ten fields were randomly selected from each sample (*n* = 4 mice per experimental group) for 4 samples. For lectin staining, Fluorescein Griffonia (Bandeiraea) Simplicifolia Lectin I (Vector Laboratories) was injected via tail vein 10 minutes before harvesting the samples. BAT or WAT tissues were finely minced with a scalpel and incubated with PBS containing Bodipy BODIPY-TR (Invitrogen) at the concentration of 1000:1. Samples were washed 3 times with PBS and mounted for further observations. The confocal microscope (LSM710; Zeiss), located at the Boston University Medical Campus Cellular Imaging Core, was used for the study. ImageJ was used to evaluate the positive area. Hypoxic conditions of BAT and WAT from mice with diet-induced obesity were also evaluated with hypoxyprobe (pimonidazole). Mice were injected with pimonidazole (60 mg/kg, i.p.) 1 hour before sacrifice, and low oxygen levels were visualized by brown staining on slides of paraffin-embedded adipose tissue using the Hypoxyprobe-1 Plus Kit (Chemicon International). Hypoxyprobe-1 is a pimonidazole hydrochloride that is used to assay for hypoxic conditions in tissues and cultured cells. It forms adducts with proteins under low oxygen concentrations (59). Four fields were randomly

selected from each sample to calculate the hypoxyprobe positive area. Several sections were generated from BAT embedded in OCT compound (frozen sections) for immunohistochemical analysis of mitochondrial membrane protein Tom20 (Santa Cruz Biotechnology Inc.) colocalizing with autophagosomal membrane protein LC3 (Cell Signaling). For vascular leak analysis, FITC-Dextran (MW4000; Sigma-Aldrich) was injected via tail vein 6 hours prior to euthanizing, and then BAT was embedded in OCT compound for further analysis. Four fields were randomly selected from each sample to calculate leak-positive area. Hif1α and β-gal expression were detected with immunohistochemistry (DAB substrate kit, Vector Labs; Hif1α antibody, Abcam; β-gal antibody; Santa Cruz Biotechnology Inc.).

Oxygen measurement. Oxygen levels of BAT were measured with the needle-type oxygen microsensor (MICROX TX3, Precision Sensing) as instructed by the manufacturer.

ELISA. VEGF-A levels were detected from WAT and BAT using an ELISA kit (R&D Systems); FFA levels were detected from BAT using an ELISA (Bio-Vision) as instructed by the manufacturer. For detecting FFA, 10–15 mg of BAT was homogenized with 200 μl of chloroform–Triton X-100 (1% Triton X-100 in pure chloroform) in a microhomogenizer, and phases were separated by centrifugation at top speed (21,130 g) in a microcentrifuge. The lower phase (organic) was collected and air dried at 50°C to remove chloroform. The dried lipids (in Triton X-100) were dissolved in 200 μl of fatty acid assay buffer for further analysis. Levels of cAMP were measured in the differentiated brown adipocyte cell line treated with hypoxic stress (1% O_2 for 24 hours) using an ELISA kit (R&D Systems). At the end of the hypoxic stress period, cells were treated with 0.1–100 μM isoprenaline hydrochloride (ISO) for 10 minutes and immediately washed in cold PBS 3 times. Cells were resuspended with 0.1 N HCL for further analysis. Some undigested wells (n = 4) were resuspended with 0.25% trypsin/EDTA solution for counting cells. The cAMP levels obtained with the ELISA kit were divided with average cell numbers per group measured and shown as pmol/10^6 cells.

RNA analysis. Interscapular BAT was collected from mice. RNA was extracted using the RNeasy Lipid Tissue Mini Kit (QIAGEN), and cDNA was generated with the QuantiTect Reverse Transcription Kit (QIAGEN) according to the manufacturer's instructions. Real-time PCR was performed using the ViiA TM7 Real Time PCR System (Applied Biosystems) with the SYBR Green Real Time PCR Master Mixes (Applied Biosystems) according to the manufacturer's instructions. For most transcripts, the relative levels of mRNA were determined using the ΔΔCT method, normalizing to *Actb*. For *Adrb1* and *Adrb3*, copy number was determined by generating a 6-point standard curve using plasmid-encoded Adrb1 (MC216246; Origene) or Adrb3 (MC208113; Origene).

Primers and their sequences are as follows: *Vegfa*: 5′-TCTCTTGGGT-GCACTGGACC-3′, 5′-GTTACAGCAGCCTGCACAGC-3′; *Ucp-1*: 5′-CAACTTGGAGGAAGAGATACTGAACAT-3′, 5′-TTTGGTTGGTTTTATTCGTGGTC-3′; *Kdr*: 5′-CCCCAAATTCCAT-TATGACAA-3′, 5′-CGGCTCTTTCGCTTACTGTT-3′; *ND5*: 5′-AGCATTC-GGAAGCATCTTTG-3′, 5′-TTGTGAGGACTGGAATGCTG-3′; *Ndufa*: 5′-AGACGCATCTCTGGTGTCAA-3′, 5′-GCCAGGAAAATGCTTCCT-TA-3′; *Atp5a*: 5′-TGCATGGACTGAGGAACG-3′, 5′-CCAAGTTCAGGGA-CATACCC-3′; *Ppargc1a*: 5′-GAAAGGGCCAAACAGAGAGA-3′, 5′-GTAAAT-CACACGGCGCTCTT-3′; *Map1lc3b*: 5′-CCCCACCAAGATCCCAGT-3′, 5′-CGCTCATGTTCACGTGGT-3′; *Bnip3*: 5′-CCTGTCGCAGTTGGGTTC-3′, 5′-GAAGTGCAGTTCTACCCAGGAG-3′; *Emr1*: 5′-CCTGGACGAATCCTGT-GAAG-3′, 5′-GGTGGGACCACAGAGAGTTG-3′; *Tnf*: 5′-TCTTCTCATTCCT-GCTTGTGG-3′, 5′-GGTCTGGGCCATAGAACTGA-3′; *Ccl2*: 5′-CATC-CACGTGTTGGCTCA-3′, 5′-GATCATCTTGCTGGTGAATGAGT-3′; *Actb*: 5′-CTAAGGCCAACCGTGAAAAG-3′, 5′-ACCAGAGGCATACAGGGACA-3′; *Adrb1*: 5′-CATCATGGGTGTGTTCACG-3′, 5′-GGAAAGCCTTCACCAC-GTT-3′; *Adrb3*: 5′-CAGCCAGCCCTGTTGAAG-3′, 5′-CCTTCATAGCCAT-

CAAACCTG-3′; *Eln*: 5′-TGGAGCAGGACTTGGAGGT-3′, 5′-CCTCCAG-CACCATACTTAGCA-3′; and *Lox*: 5′-CAGGCTGCACAATTTCACC-3′, 5′-CAAACACCAGGTACGGCTTT-3′.

Western blot analysis. Whole-cell lysates were prepared in lysis buffer (RIPA Buffer with Halt Protease and Phosphatase Inhibitor Cocktail; Thermo Scientific). The lysates (20–50 μg) were resolved by SDS-PAGE. The mitochondrial fraction was extracted using a Mitochondria Isolation Kit (Thermo Scientific) according to the manufacturer's instructions. Proteins were transferred to a PVDF membrane (Bio-Rad), which was incubated with the primary antibody followed by anti-rabbit immunoglobulin-G conjugated with horseradish peroxidase (Cell Signaling). Specific proteins were detected by enhanced chemiluminescence (Amersham). The primary antibodies used for Western blotting were as follows: LC3A/B, GAPDH (14C10), Myc-Tag, α/β-tubulin, PINK1, CoxIV, ubiquitin, phospho-PKA C (Thr197), PKA C-α (Cell Signaling), VEGF (A-20) (Santa Cruz Biotechnology Inc.), Parkin, anti–β1-adrenergic receptor (Abcam), and anti–β3-adrenergic receptor antibody (Abcam).

Cell line. The brown preadipocyte cell line was a gift from C. Ronald Kahn (Joslin Diabetes Center and Harvard Medical School, Section on Integrative Physiology and Metabolism, Boston, Massachusetts, USA) (60). It was extracted from WT FVB mice and immortalized by infection with the retroviral vector pBabe encoding SV40T antigen. Cells were cultured with high-glucose DMEM plus 10% FBS plus PS and differentiated as previously described (61). Fully differentiated brown adipocytes (after 10 days of differentiation) were used for further analysis. In some experiments, cells were infected with ad-*Hif1a* for 48 hours. In some experiments, palmitic acid (500 μM) was added to the 1% albumin medium.

Hypoxia chamber methods. BAT extracted from WT C57BL/6 mice was cultured in DMEM (high glucose) and exposed to hypoxic conditions (1% O_2) using a hypoxia chamber (Stemcell Technologies) according to the manufacturer's instructions. Brown adipocyte cell lines were also cultured under hypoxic conditions. The time course for hypoxic exposure ranged from 6 to 24 hours according to the assay. MitoSOX (1 μM, 10 minutes), Mito-Tracker Green FM (MitoGreen) (100 nM, 45 minutes), and MitoTracker Red CM-H2Xros (MitoRed) (200 nM, 45 minutes) (Invitrogen) were used according to the manufacturer's instructions and visualized by confocal microscopy using a Zeiss LSM710. Mito Red–positive area or number of MitoSOX-positive mitochondria were measured on 10 random fields selected from each sample (n = 4 mice per experimental group) for 4 samples observed at ×1000 magnification.

FACS analysis. The mitochondrial fraction was extracted using a Mitochondria Isolation Kit (Thermo Scientific) according to the manufacturer's instructions. Isolated mitochondria were resuspended with mitochondria assay solution containing sucrose (70 mM), mannitol (220 mM), KH_2PO_4 (10 mM), $MgCl_2$ (5 mM), EGTA (1 mM), FFA BSA (0.2%), PIPES pH 6.8 (25 mM), BES pH 7.0 (25 mM), and MOPS pH 7.2 (25 mM) adjusted to pH 7.4 with KOH and stained with MitoRed (500 nM) or MitoSOX (5 μM) (Invitrogen). Flow cytometry was performed using an LSRII (BD). For MitoRed detection, we used a YG561nm laser and a 610/20 filter. For MitoSOX detection, we used a 488-nm laser and a 585/42 filter. Carbonyl cyanide m-chlorophenylhydrazone (CCCP) (200 μM) was used as an uncoupler to depolarize mitochondria. MitoSOX or MitoRed signals were quantified, with the geometric mean analyzed with FlowJo.

Radioligand binding assay. Fully differentiated brown adipocytes were cultured under hypoxic conditions for 24 hours. [^{3}H]-(-)-CGP-12177 (PerkinElmer Life and Analytical Sciences) was used at a concentration of 0.1-2.5 nM when examining the high-affinity β1-adrenoreceptor interaction and at 0.1–100 nM for the low-affinity β3-adrenoreceptor interaction. The β1-adrenoreceptor antagonist CGP20712A (10 μM; Sigma-Aldrich) or the β3-adrenoreceptor antagonist SR59230A (10 μM; Sigma-Aldrich)

was used to define specific binding. Reactions were terminated by aspiration, and cells were washed twice with cold PBS and digested with 0.2 M NaOH. The contents of the wells were transferred to vials with scintillation buffer (Ecolite(+) Liquid Scintillation Fluid; MP Biomedicals) and radioactivity measured using an analyzer (Tri-Carb 2900TR; PerkinElmer Life and Analytical Sciences). Unused wells ($n = 5$) were resuspended with 0.25% Trypsin/EDTA solution for counting cells. The radioactivity levels obtained with the scintillation analyzer were divided with average cell numbers per group measured and presented as fmol $\times 10^{-5}$/cell. A nonlinear curve was obtained with nonlinear curve fitting (GraphPad Prism version 6; GraphPad Software Inc).

Statistics. Data are shown as the mean ± SEM. Differences between groups were examined by 2-tailed Student's *t* test or 2-way ANOVA for comparisons among multiple groups. For all analyses, $P < 0.05$ was considered statistically significant.

Study approval. The Institutional Animal Care and Use Committee (IACUC) of Boston University approved all animal study procedures.

Address correspondence to: Kenneth Walsh, Molecular Cardiology/Whitaker Cardiovascular Institute, Boston University School of Medicine, 715 Albany Street, W611, Boston, Massachusetts 02118, USA. Phone: 617.414.2392; Fax: 617.414.2391; E-mail: kxwalsh@bu.edu.

1. Chechi K, Carpentier AC, Richard D. Understanding the brown adipocyte as a contributor to energy homeostasis. *Trends Endocrinol Metab*. 2013; 24(8):408–420.
2. Tseng YH, Cypess AM, Kahn CR. Cellular bioenergetics as a target for obesity therapy. *Nat Rev Drug Discov*. 2010;9(6):465–482.
3. Seale P, Lazar MA. Brown fat in humans: turning up the heat on obesity. *Diabetes*. 2009;58(7):1482–1484.
4. Cypess AM, et al. Identification and importance of brown adipose tissue in adult humans. *N Engl J Med*. 2009;360(15):1509–1517.
5. Bartelt A, et al. Brown adipose tissue activity controls triglyceride clearance. *Nat Med*. 2011; 17(2):200–205.
6. Hamann A, Flier JS, Lowell BB. Decreased brown fat markedly enhances susceptibility to diet-induced obesity, diabetes, and hyperlipidemia. *Endocrinology*. 1996;137(1):21–29.
7. Nedergaard J, Bengtsson T, Cannon B. Unexpected evidence for active brown adipose tissue in adult humans. *Am J Physiol Endocrinol Metab*. 2007; 293(2):E444–E452.
8. Pfannenberg C, et al. Impact of age on the relationships of brown adipose tissue with sex and adiposity in humans. *Diabetes*. 2010;59(7):1789–1793.
9. Stanford KI, et al. Brown adipose tissue regulates glucose homeostasis and insulin sensitivity. *J Clin Invest*. 2013;123(1):215–223.
10. Sun K, et al. Dichotomous effects of VEGF-A on adipose tissue dysfunction. *Proc Natl Acad Sci USA*. 2012; 109(15):5874–5879.
11. Sung HK, et al. Adipose vascular endothelial growth factor regulates metabolic homeostasis through angiogenesis. *Cell Metab*. 2013;17(1):61–72.
12. Elias I, et al. Adipose tissue overexpression of vascular endothelial growth factor protects against diet-induced obesity and insulin resistance. *Diabetes*. 2012;61(7):1801–1813.
13. Hosogai N, et al. Adipose tissue hypoxia in obesity and its impact on adipocytokine dysregulation. *Diabetes*. 2007;56(4):901–911.
14. Pasarica M, et al. Reduced adipose tissue oxygenation in human obesity: evidence for rarefaction, macrophage chemotaxis, and inflammation without an angiogenic response. *Diabetes*. 2009; 58(3):718–725.
15. Rausch ME, Weisberg S, Vardhana P, Tortoriello DV. Obesity in C57BL/6J mice is characterized by adipose tissue hypoxia and cytotoxic T-cell infiltration. *Int J Obes (Lond)*. 2008;32(3):451–463.
16. Ye J, Gao Z, Yin J, He Q. Hypoxia is a potential risk factor for chronic inflammation and adiponectin reduction in adipose tissue of ob/ob and dietary obese mice. *Am J Physiol Endocrinol Metab*. 2007; 293(4):E1118–E1128.
17. Yin J, Gao Z, He Q, Zhou D, Guo Z, Ye J. Role of hypoxia in obesity-induced disorders of glucose and lipid metabolism in adipose tissue. *Am J Physiol Endocrinol Metab*. 2009;296(2):E333–E342.
18. Miranda M, et al. Relation between human LPIN1, hypoxia and endoplasmic reticulum stress genes in subcutaneous and visceral adipose tissue. *Int J Obes (Lond)*. 2010;34(4):679–686.
19. Halberg N, et al. Hypoxia-inducible factor 1alpha induces fibrosis and insulin resistance in white adipose tissue. *Mol Cell Biol*. 2009;29(16):4467–4483.
20. He Q, Gao Z, Yin J, Zhang J, Yun Z, Ye J. Regulation of HIF-1{alpha} activity in adipose tissue by obesity-associated factors: adipogenesis, insulin, and hypoxia. *Am J Physiol Endocrinol Metab*. 2011; 300(5):E877–E885.
21. Voros G, Maquoi E, Demeulemeester D, Clerx N, Collen D, Lijnen HR. Modulation of angiogenesis during adipose tissue development in murine models of obesity. *Endocrinology*. 2005;146(10):4545–4554.
22. Kolonin MG, Saha PK, Chan L, Pasqualini R, Arap W. Reversal of obesity by targeted ablation of adipose tissue. *Nat Med*. 2004;10(6):625–632.
23. Xue Y, et al. Hypoxia-independent angiogenesis in adipose tissues during cold acclimation. *Cell Metab*. 2009;9(1):99–109.
24. Zhang J, Wang Y, Gao Z, Yun Z, Ye J. Hypoxia-inducible factor 1 activation from adipose protein 2-cre mediated knockout of von Hippel-Lindau gene leads to embryonic lethality. *Clin Exp Pharmacol Physiol*. 2012;39(2):145–150.
25. Makowski L, et al. Lack of macrophage fatty-acid-binding protein aP2 protects mice deficient in apolipoprotein E against atherosclerosis. *Nat Med*. 2001;7(6):699–705.
26. Chandel NS, Maltepe E, Goldwasser E, Mathieu CE, Simon MC, Schumacker PT. Mitochondrial reactive oxygen species trigger hypoxia-induced transcription. *Proc Natl Acad Sci USA*. 1998; 95(20):11715–11720.
27. Guzy RD, et al. Mitochondrial complex III is required for hypoxia-induced ROS production and cellular oxygen sensing. *Cell Metab*. 2005;1(6):401–408.
28. Scherz-Shouval R, Elazar Z. ROS, mitochondria and the regulation of autophagy. *Trends Cell Biol*. 2007; 17(9):422–427.
29. Chen Y, Dorn GW 2nd. PINK1-phosphorylated mitofusin 2 is a Parkin receptor for culling damaged mitochondria. *Science*. 2013;340(6131):471–475.
30. Sun K, Halberg N, Khan M, Magalang UJ, Scherer PE. Selective inhibition of hypoxia-inducible factor 1alpha ameliorates adipose tissue dysfunction. *Mol Cell Biol*. 2013;33(5):904–917.
31. Bellot G, et al. Hypoxia-induced autophagy is mediated through hypoxia-inducible factor induction of BNIP3 and BNIP3L via their BH3 domains. *Mol Cell Biol*. 2009;29(10):2570–2581.
32. Fredriksson JM, Lindquist JM, Bronnikov GE, Nedergaard J. Norepinephrine induces vascular endothelial growth factor gene expression in brown adipocytes through a beta -adrenoreceptor/cAMP/protein kinase A pathway involving Src but independently of Erk1/2. *J Biol Chem*. 2000; 275(18):13802–13811.
33. Lambert GW, Straznicky NE, Lambert EA, Dixon JB, Schlaich MP. Sympathetic nervous activation in obesity and the metabolic syndrome — causes, consequences and therapeutic implications. *Pharmacol Ther*. 2010;126(2):159–172.
34. Marette A, Geloen A, Collet A, Bukowiecki LJ. Defective metabolic effects of norepinephrine and insulin in obese Zucker rat brown adipose tissue. *Am J Physiol*. 1990;258(2 pt 1):E320–E328.
35. Lowell BB, Flier JS. Brown adipose tissue, beta 3-adrenergic receptors, and obesity. *Annu Rev Med*. 1997;48:307–316.
36. Robidoux J, Martin TL, Collins S. Beta-adrenergic receptors and regulation of energy expenditure: a family affair. *Annu Rev Pharmacol Toxicol*. 2004; 44:297–323.
37. Mottillo EP, Granneman JG. Intracellular fatty acids suppress beta-adrenergic induction of PKA-targeted gene expression in white adipocytes. *Am J Physiol Endocrinol Metab*. 2011;301(1):E122–E131.
38. Asano A, Morimatsu M, Nikami H, Yoshida T, Saito M. Adrenergic activation of vascular endothelial growth factor mRNA expression in rat brown adipose tissue: implication in cold-induced

angiogenesis. *Biochem J.* 1997;328(pt 1):179–183.

39. Tonello C, et al. Role of sympathetic activity in controlling the expression of vascular endothelial growth factor in brown fat cells of lean and genetically obese rats. *FEBS Lett.* 1999;442(2–3):167–172.

40. Goossens GH, et al. Increased adipose tissue oxygen tension in obese compared with lean men is accompanied by insulin resistance, impaired adipose tissue capillarization, and inflammation. *Circulation.* 2011;124(1):67–76.

41. Lijnen HR, et al. Impaired adipose tissue development in mice with inactivation of placental growth factor function. *Diabetes.* 2006;55(10):2698–2704.

42. Rupnick MA, et al. Adipose tissue mass can be regulated through the vasculature. *Proc Natl Acad Sci U S A.* 2002;99(16):10730–10735.

43. Brakenhielm E, et al. Angiogenesis inhibitor, TNP-470, prevents diet-induced and genetic obesity in mice. *Circ Res.* 2004;94(12):1579–1588.

44. Brakenhielm E, et al. Adiponectin-induced antiangiogenesis and antitumor activity involve caspase-mediated endothelial cell apoptosis. *Proc Natl Acad Sci U S A.* 2004;101(8):2476–2481.

45. Yilmaz M, Hotamisligil GS. Damned if you do, damned if you don't: the conundrum of adipose tissue vascularization. *Cell Metab.* 2013;17(1):7–9.

46. Hodson L, Humphreys SM, Karpe F, Frayn KN. Metabolic signatures of human adipose tissue hypoxia in obesity. *Diabetes.* 2013;62(5):1417–1425.

47. Dutta A, Popel AS. A theoretical analysis of intracellular oxygen diffusion. *J Theor Biol.* 1995; 176(4):433–445.

48. Choi AM, Ryter SW, Levine B. Autophagy in human health and disease. *N Engl J Med.* 2013;368(7):651–662.

49. Yang L, Li P, Fu S, Calay ES, Hotamisligil GS. Defective hepatic autophagy in obesity promotes ER stress and causes insulin resistance. *Cell Metab.* 2010; 11(6):467–478.

50. Singh R, et al. Autophagy regulates adipose mass and differentiation in mice. *J Clin Invest.* 2009; 119(11):3329–3339.

51. Zhang Y, Goldman S, Baerga R, Zhao Y, Komatsu M, Jin S. Adipose-specific deletion of autophagy-related gene 7 (atg7) in mice reveals a role in adipogenesis. *Proc Natl Acad Sci U S A.* 2009; 106(47):19860–19865.

52. Madamanchi NR, Runge MS. Redox signaling in cardiovascular health and disease. *Free Radic Biol Med.* 2013;61C:473–501.

53. Kubli DA, Gustafsson AB. Mitochondria and mitophagy: the yin and yang of cell death control. *Circ Res.* 2012;111(9):1208–1221.

54. Bostrom P, et al. A PGC1-alpha-dependent myokine that drives brown-fat-like development of white fat and thermogenesis. *Nature.* 2012; 481(7382):463–468.

55. Ohno H, Shinoda K, Spiegelman BM, Kajimura S. PPARgamma agonists induce a white-to-brown fat conversion through stabilization of PRDM16 protein. *Cell Metab.* 2012;15(3):395–404.

56. Wu J, Cohen P, Spiegelman BM. Adaptive thermogenesis in adipocytes: is beige the new brown? *Genes Dev.* 2013;27(3):234–250.

57. Nedergaard J, Cannon B. UCP1 mRNA does not produce heat. *Biochim Biophys Acta.* 2013; 1831(5):943–949.

58. Gerber HP, et al. VEGF is required for growth and survival in neonatal mice. *Development.* 1999; 126(6):1149–1159.

59. Shabsigh A, et al. Biomarker analysis demonstrates a hypoxic environment in the castrated rat ventral prostate gland. *J Cell Biochem.* 2001;81(3):437–444.

60. Klein J, Fasshauer M, Ito M, Lowell BB, Benito M, Kahn CR. beta(3)-adrenergic stimulation differentially inhibits insulin signaling and decreases insulin-induced glucose uptake in brown adipocytes. *J Biol Chem.* 1999;274(49):34795–34802.

61. Fasshauer M, Klein J, Kriauciunas KM, Ueki K, Benito M, Kahn CR. Essential role of insulin receptor substrate 1 in differentiation of brown adipocytes. *Mol Cell Biol.* 2001;21(1):319–329.